https://doi.org/10.1016/j.matchemphys.2020.123555

Impact of microalloying element Ga on the glass-forming ability (GFA), mechanical properties and corrosion behavior of Mg-Zn-Ca bulk metallic glass

Wei Zai[a], H.C. Man[b], Yingchao Su[c], Guangyu Li[a,*], Jianshe Lian[a]

[a] Key Laboratory of Automobile Materials, Ministry of Education, College of Materials Science and Engineering, Jilin University, Changchun 130025, China

[b] Department of Industrial & Systems Engineering, The Hong Kong Polytechnic University, Hong Kong, China

[c] Department of Biomedical Engineering, Stony Brook University, Stony Brook, NY, 11794, USA.

Abstract

By virtue of its high corrosion resistance and desirable mechanical properties, Mg-based bulk metallic glass (BMG) is a promising candidate material for the biodegradable implants ~~material~~. To investigate the impact of microalloying element Ga on the glass-forming ability (GFA) and its effect on the mechanical properties and corrosion behavior of Mg-Zn-Ca BMG, a series alloys of $(Mg_{66}Zn_{30}Ca_4)_{100-x}Ga_x$ ($0 \leq x \leq 1.25$) BMG were synthesized and investigated in this study. The critical diameter of $Mg_{66}Zn_{30}Ca_4$ BMG is about 3.5 mm, and an appropriate addition of Ga (1.0 at.%) can improve the critical diameter (D_c) to 5 mm. Meanwhile, the approximate addition of Ga ~~can slightly~~ improves the fracture strength of Mg-Zn-Ca BMG from 651 MPa to 752 MPa. The addition of Ga can also help forming passive ~~corrosion product~~ film on the substrate and therefore improves the corrosion resistance.

* Corresponding author. E-mail address: guangyu@jlu.edu.cn (G. Li).

1. Introduction

During the past decades, bulk metallic glasses (BMG) have gained increasing attention from materials scientists and engineers as one category of new important materials [1]. From the first report of a metallic glass fabricated by Pol Duwez and his colleagues in 1960 [2], a great number of ~~categories~~ BMG systems have been designed and fabricated ~~found in the researches of metallic glass~~. ~~But~~ The first ~~kind~~ system of metallic glass (Au-Si alloy) needs a very rapid cool-down rate, approaching a million degrees per second, in fabrication [3]. Since 1988, many ~~kinds~~ systems of bulk metallic glasses have been ~~discovered~~ studied, such as the Mg-based, La-based, Zr-based, Fe-based, Pd-based BMG [4] and so on. Some ~~categories~~ systems of metallic glass have a great glass-forming ability (GFA). $Pd_{40}Cu_{30}Ni_{10}P_{20}$ metallic glass can even have a critical diameter (D_c) up to 72 mm [5]. At the same time, metallic glasses have very outstanding properties such as the highest elastic limit among metallic materials (up to twice that of common metals), high strength (approaching the theoretical limiting strength of that kind of alloy) and high corrosion resistance (without crystal and grain boundaries and localized corrosion), making metallic glass ~~become~~ a very promising class of materials.

Although fabricating BMGs with diameters of several centimeters is already successful, some toxic elements must be ~~brought in~~ used in the meantime. ~~Just like~~ For Mg-based BMGs, it ~~will be~~ is difficult to improve the D_c to over 10 mm without the addition of Ni [6], Be [7] or Cu [8]. In some systems ~~even can~~ only ~~get~~ amorphous ribbons with the thickness of dozens of microns can be achieved. The small critical diameters ~~and the low GFA~~ of BMGs in general and the low GFA in many systems ~~still~~ significantly restrict the potential applications in the medical field. Therefore improving

the GFA and critical sizes of BMGs to satisfy the requirement of geometric size is still the main challenge of further ~~exploring and~~ development of BMG in biomedical applications [9].

Owing to the increased number of the aging population and the requirement for higher living standards, large demands of biomaterials are expected ~~to come~~ in the future [9][10]. Mg-based metallic glasses are now receiving increased attention from the medical industry as one category of new important materials for biomedical applications. Physical and mechanical properties such as low density, close matching of elastic modulus with the cortical bone, and biological properties such as bio-compatibility, bio-degradability, and bio-resorbability, are some of the reasons contributing to their recognition as promising materials in the biomedical field [11]. Unlike their crystalline counterparts, they are single-phased and ~~chemically~~ homogenous systems with the absence of microstructural defects such as grain boundaries, dislocations, and precipitates [12][13]. It motivates attempts of application of these materials for producing resorbable orthopedic implants according to the new concept of implants with controlled and predictable resorption [14]. Gu et al. [15] and Zberg ~~B~~ et al. [16] ~~et al~~ demonstrated that Mg-Zn-Ca BMGs have more uniform corrosion morphology, much lower corrosion rates, and higher cell viability than conventional crystalline pure Mg. Some categories of Mg-based BMG have a great glass-forming ability, for example, $Mg_{54}Cu_{26.5}Ag_{8.5}Gd_{11}$ ~~(fabricated by Institute of Metal Research)~~, and have a D_c up to 25 mm [17]. However, Mg-Zn-Ca, the most promising Mg-based BMG system for biomedical applications ~~which received special research attention across the scientific community~~ ~~is still have~~ has a limited GFA [16][15]. Ryszard et al. [14] demonstrated that the content of Zn and Ca would directly

affect ~~impact~~ the GFA of Mg-Zn-Ca BMG. Without other elements added to Mg-Zn-Ca BMG, the maximum D_c is about 4 mm [14]. To improve the performance of Mg-Zn-Ca BMG, there were attempts to add alloying elements ~~have been investigated to improve the property of~~ to the Mg-Zn-Ca system, such as Ag [18], Pd [19], Cu [20], Sr [21]. The addition of Ag from 1% to 3% decreased the D_c of Mg-Zn-Ca BMG from 2 mm to 1 mm, but it improved the corrosion resistance. Only the element Sr would increase the D_c to about 6 mm [21]. *[How abou Pd and Cu?]*

In this study, to improve the properties of Mg-Zn-Ca BMG, a series of $(Mg_{66}Zn_{30}Ca_4)_{100-x}Ga_x$ ($0 \leq x \leq 1.25$) BMG were synthesized and investigated. The microstructure, GFA, mechanical properties, corrosion resistance and thermal stability of Mg-Zn-Ca-Ga BMG were evaluated.

2. Experimental

2.1 Materials preparation

Pure Mg (99.9%), Zn (99.9%), binary Mg-30Ca master alloy and pure Ga (99.9%) were used as starting materials. Then ~~all alloys~~ mixtures with different proportions were melted in a graphite crucible placed in an induction furnace under ~~an ordinary atmosphere with~~ a high purity argon (99.999%) atmosphere. ~~Graphite crucible was used as the melting vessel to prepare~~ ~~the~~ Master alloys with varying Ga content $(Mg_{66}Zn_{30}Ca_4)_{100-x}Ga_x$ (x= 0, 0.25, 0.5, 0.75, 1 and 1.25) were prepared. Every master alloy was re-melted more than three times to ensure the compositional homogeneity. Re-melted ingots were then cut into pieces and spray-casted into a copper-mold to get cylindrical samples with diameters of 2, 3.5 and 5 mm, respectively. Metallic glass

ribbons with 40 μm in thickness and 5 mm in width were also prepared by a single roller melt spinning process at a wheel speed of 40 m/s.

2.2. Microstructure characterization and mechanical properties

Cross-sectional surfaces of the as-cast cylindrical samples were analyzed by X-ray diffraction (XRD) using a Rigaku Dymax diffractometer with CuKα radiation (λ = 1.5405 Å) and scanning-electron microscopy (SEM, Tescan VEGA3). Differential scanning calorimetry (DSC, Perkin-Elmer) was also used to characterize the natures of different amorphous samples, with a heating rate of 40 K/min in an ultra-high purity Ar atmosphere. ~~And~~ The weight of every sample prepared for DCS was 10 to 20 mg. The MTS 810 servo-hydraulic material testing machine was used to ~~process~~ in the uniaxial compression test performed at a constant strain rate of 1×10^{-4} s^{-1}at room temperature. The as-cast cylindrical samples with 3.5 mm in diameter and 7 mm in length were used ~~to conduct~~ in the compression test.

2.3. Electrochemical tests

Mg-Zn-Ca-Ga metallic glass ribbons with the 1 cm^2 exposed surface were used to conduct the electrochemical tests in Hanks' simulated body fluid solution [22][36] (the ~~specific~~ composition is listed in Table TTT1). The Versa STAT3 electrochemical workstation (Princeton Applied Research) with a standard three-electrode configuration was used to carry out the electrochemical tests. Platinum plate with an area of about 1 cm^2 and saturated calomel electrode (SCE) ~~are set~~ served as the counter electrode (CE) and reference electrode (RE), respectively. ~~Every tested sample was immersed in Hanks' solution to monitor the change of~~ The open-circuit potential (OCP) was recorded for 60 min ~~to get into stable corrosion status. After 60 min OCP test,~~ before

electrochemical impedance spectroscopy (EIS) measurement was conducted from 100 kHz to 0.05 Hz with an amplitude of 5 mV versus the OCP ~~of each sample~~. ~~And~~ The EIS result was fitted using the ZSimpWin software. ~~In the end~~ Subsequently the potential dynamic polarization (PDP) test was carried out from -0.5 V (vs. OCP) toward the anodic direction at a scan rate of 1 mV/s. The ~~free~~ corrosion potential (E_{corr}) and the ~~free~~ corrosion current density (I_{corr}) were ~~calculated~~ extracted from the PDP curves.

Table TTT1

Composition of Hanks' solution [36].

Chemical	NaCl	KCl	$NaHCO_3$	$MgSO_4 \cdot 7H_2O$	Glucose	$CaCl_2$	KH_2PO_4	$Na_2HPO_4 \cdot 2H_2O$
Mass (g/L)	8	0.4	0.35	0.2	1	0.14	0.06	0.06

2.4 Immersion test

To evaluate the corrosion resistance of all Mg-Zn-Ca-Ga metallic glass samples, Mg-based metallic glass ribbons with an exposed area of $1cm^2$ were immersed into 200 mL Hanks' solution for the immersion test. The solution temperature ~~of Hanks' solution~~ was kept at the constant of 37 ℃ ~~using a water bath~~. [*What was the immersion period?*] After the immersion test, the corrosion surfaces of different metallic glass samples were investigated by SEM.

3. Results

3.1 Microstructure characterization

As shown in Fig. XXX1, the XRD patterns of sample Ga0 with a diameter of 3.5 mm and Ga1.00 with a diameter of 5 mm exhibit a broad amorphous peak at about $2\theta = 37°$ without any obvious typical crystalline peaks. On the other hand, the addition of 0.25 at.% and 0.5 at.% Ga ~~directly~~ obviously decreases the GFA of Mg-Zn-Ca BMG; Ga0.25

and Ga0.50 exhibit typical crystalline peaks of Mg, MgZn and $Mg_{51}Zn_{20}$ phases. With the increase of the element Ga, two broad peaks at about 2θ = 36.6° and 2θ = 39.2° replace the sharp and distinct crystalline peaks on the XRD patterns of sample Ga0.75 with a diameter of 5 mm. When the addition of Ga is 1 at.%, Mg-Zn-Ca-Ga BMG has the maximum GFA with ~~about~~ D_c of about 5 mm. When the addition of Ga up to 1.25 at.%, ~~the~~ D_c ~~of Ga1.25~~ decreases to about 3.5 mm and indistinct crystalline peaks similar to the major peaks of Mg and $Mg_{51}Zn_{20}$ appear respectively at about 2θ = 36.6° and 2θ = 39.2° in the XRD patterns.

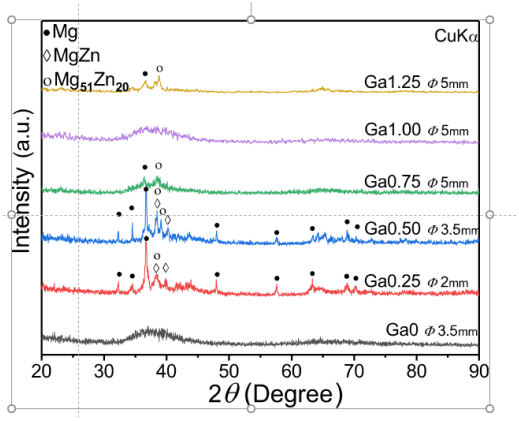

Fig. XXX1. XRD patterns of metallic glass samples ~~were got~~ acquired on the cross-sections of six different as-cast cylindrical alloys (Ga0, Ga0.25, Ga0.5, Ga0.75, Ga1.0, Ga1.25) with different diameters.

SEM (backscattered electron) images of the center of different metallic glass samples were presented in Fig. XXX2. Without the addition of Ga, ~~only~~ a few crystals ~~particles~~ are observed in the center of sample Ga0 (3.5 mm) in Fig. XXX2(a). When only 0.25 at.% of Ga was added the GFA decreased obviously and a large number of crystals are observed in the center as shown in Fig. XXX2(b). When the addition of Ga is up to 0.75 at.% and 1.0 at.%, ~~only~~ a few crystal particles appear in the center of Ga0.75 with a

diameter of 3.5 mm and Ga1.0 with a diameter of 5 mm. With the further addition of Ga, obvious crystal phases were formed in the center of Ga1.25 with a diameter of 5 mm. *[Please note the consistency of the backscattered electron SEM results and the XRD results]*

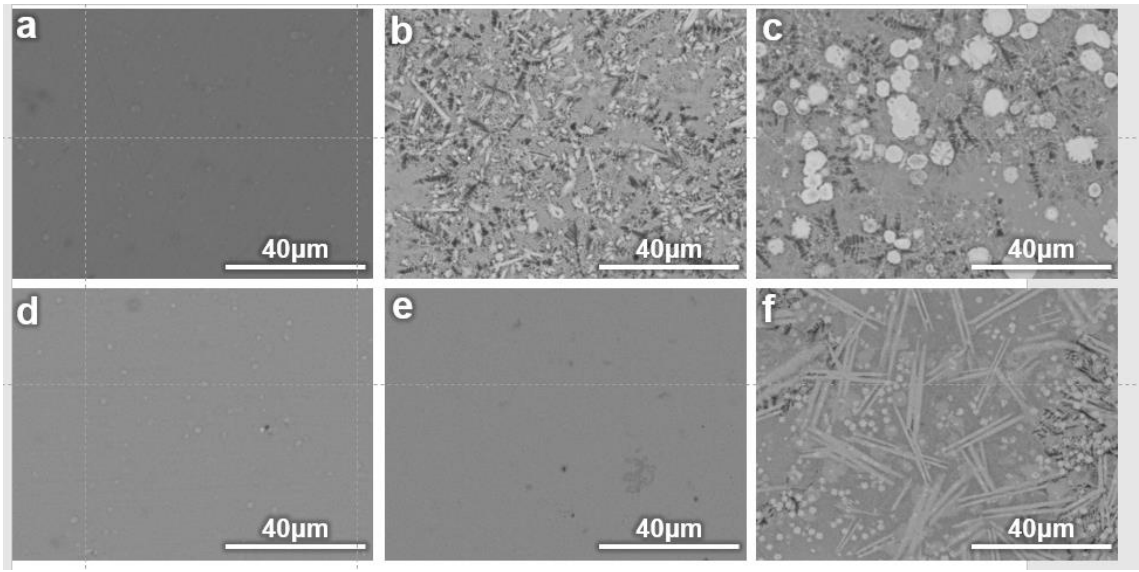

Fig. XXX2. SEM (backscattered electron) images of the center of as-casted samples: (a) Ga0 (Φ 3.5mm), (b) Ga0.25 (Φ 2mm), (c) Ga0.5(Φ 3.5mm), (d) Ga0.75 (Φ 3.5mm), (e) Ga1.0 (Φ 5mm), (f) Ga1.25 (Φ 5mm)

Fig.XXX3(a)(b) shows the DSC curves of all metallic glass samples, and the corresponding results ~~and the~~ of thermal parameters are listed in Table TTT2, including T_g (glass transition temperature), T_x (crystallization temperature), T_m (melting temperature), T_l (liquidus temperature), T_x-T_g (ΔT_x, supercooled liquid range), T_l-T_m (solid and liquid range), T_g/T_l (T_{rg}, reduced glass transition temperature), and the parameter γ defined by Eq. (1). The values of ΔT_x, T_l-T_m, T_g/T_l and γ are commonly used as the indicators of GFA [21,23-25].

$$\gamma = T_x / (T_g + T_l) \quad (1)$$

Endothermic ~~reactions~~ process corresponding to glass transition and exothermic ~~reaction~~ process corresponding to the crystallization of all alloys are displayed in Fig. XXX3(a). Sample Ga0 shows a clear glass transition process at 359 K. Across the supercooled liquid region, consequent crystallization peaks appear~~ed~~ on the DSC curve. With the increase of Ga addition, T_g does not have an obvious ~~variation~~ change and ~~keeps~~ remains at about 358 K. On the other hand T_x firstly decreases from 378 K to 375 K with only an addition of 0.25 at.% Ga. Then T_x reaches to the minimum ~~volume~~ value 372 K ~~with the addition of~~ at 0.5 at.% Ga. When the addition of Ga increases to 0.75, 1.0 and 1.25 at.%, the T_x of Ga0.75, Ga1.0 and Ga1.25 increases to 378 K, 378 K and 376 K. As Inoue postulated [3], the stability and GFA of BMG correlates with the width of the supercooled region T_x-T_g (ΔT_x). As is shown in Fig. XXX3(a) and Table TTT2, the addition of alloying element Ga affects the ΔT_x and results in the change of GFA and D_c of Mg-Zn-Ca-Ga BMGs.

The DSC curves of the melting behavior of Mg-Zn-Ca-Ga metallic glasses are presented in Fig. XXX3(b). With the variation of Ga addition, ~~the values of~~ T_m only ~~have~~ changes slightly, while T_l fluctuates dramatically as indicated by the down-arrows in Fig. XXX3(b). Besides, it is noticed that, because of the dramatic fluctuation of T_l, the value of T_g/T_l changes accordingly and directly ~~impacts~~ affects the D_c of different alloys simultaneously. As ~~Li Yi~~ Lu et al. [26] indicated, ~~in terms of~~ because of the strong correlation between T_{rg} and GFA, T_{rg} is a ~~very~~ proper index to describe GFA. For alloys with similar components, the greater the T_{rg} ~~alloys have~~, the greater the GFA will

be. It is noticed that sample Ga0.25 and Ga1.0 have the minimum and maximum T_{rg}, resulting in the minimum and maximum D_c of about 0.5 mm and 5 mm respectively.

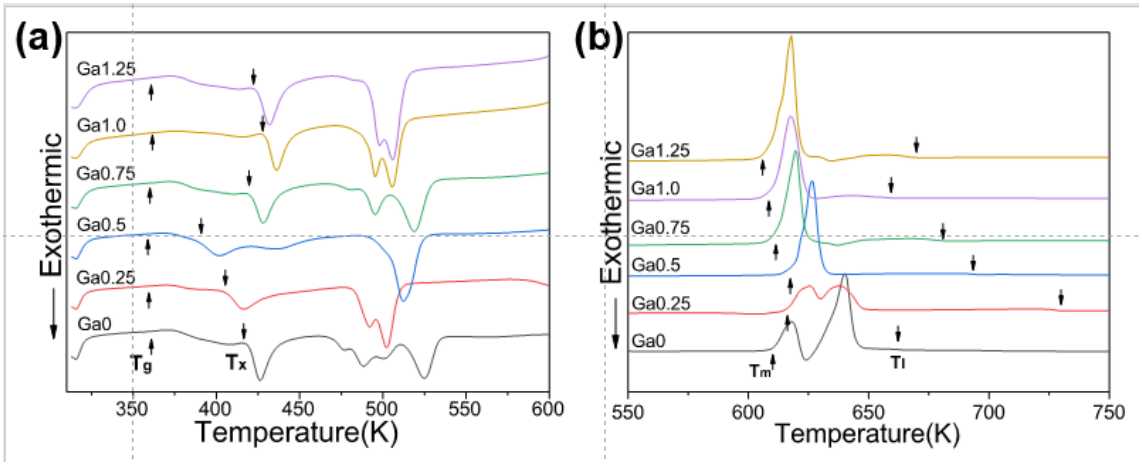

Fig. XXX3 DSC curves of Mg-based metallic glasses $(Mg_{68}Zn_{28}Ca_4)_{100-x}Ga_x$ (x = 0, 0.25, 0.5, 0.75, 1.0 and 1.25 at.%).

Table TTT2

Critical diameters (D_c) for glass formation and thermal properties of $(Mg_{68}Zn_{28}Ca_4)_{100-X}Ga_x$ (x = 0, 0.25, 0.5, 0.75, 1.0 and 1.25 at.%) BMGs.

Alloys	D_c (mm)	T_g (K)	T_x (K)	T_m (K)	T_l (K)	ΔT_x (K)	T_l-T_m (K)	T_{rg} (T_g/T_l)	γ
Ga0	3.5	359	378	609	665	**19**	56	0.540	0.369
Ga0.25	0.5	358	375	614	733	**17**	119	0.489	0.343
Ga0.5	2	358	372	613	703	**14**	90	0.509	0.350
Ga0.75	3.5	359	378	606	677	**19**	71	0.530	0.364
Ga1.0	5	358	378	610	664	**20**	54	0.539	0.370
Ga1.25	3.5	358	376	604	668	**18**	64	0.536	0.366

3.3 Mechanical properties

Since the D_c values of sample Ga0.25 and Ga0.5 were only 0.5 mm and 2 mm, only samples of Ga0, Ga0.75, Ga1.0 and Ga1.25 with 3.5 mm in diameter and 7 mm in length were tested and the test results are presented in Fig. XXX4. It is obvious that with the increase of GFA (corresponding to D_c from 3.5 mm to 5 mm) the fracture

strength increased from 651 MPa to 752 MPa and this phenomenon was also reported by Karl F. Shamlaye [27]. The probable reason is that, at a certain casting diameter, ~~the~~ BMGs having higher GFA can effectively suppress the formation and growth of crystals during the casting. As the yield strength of crystalline phase is always lower than that of the corresponding amorphous phase, during the compressive test, crystalline phase in BMG may yield firstly and result in stress concentration on the phase interface. A premature fracture may occur once crack ~~sources~~ forms and grows. Therefore increasing the GFA may be a feasible way to ~~ensure~~ increase the strength and reliability of BMGs. Furthermore, the addition of the element Ga may also play a role in solution strengthening during the compressive test.

After the compressive test, the fractured surfaces of different Mg-Zn-Ca-Ga BMG samples (Ga0, Ga0.75, Ga1.0 and Ga1.25) with 3.5 mm in diameter and 7 mm in length are presented in Fig. XXX5. All samples have the typical fracture surfaces of metallic glass, on which parallel tear lines appear on the smooth fracture surfaces. By ~~the~~ analysing the compressive stress-strain curves and fracture surfaces of the BMG (Ga0, Ga0.75, Ga1.0, and Ga1.25), in the condition of amorphous phase stage [*?*], the addition of ~~element~~ Ga does not have an obvious effect on the mechanical behavior of Mg-Zn-Ca BMG.

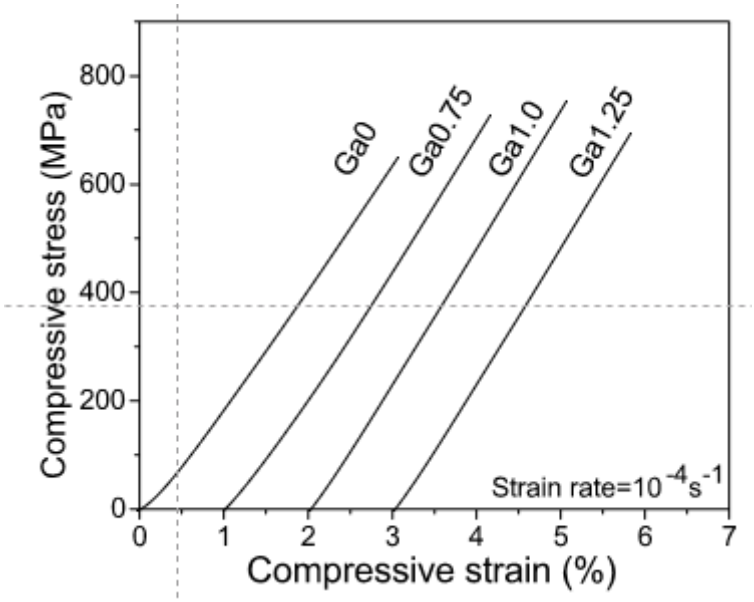

Fig. XXX4 Compressive stress-strain curves of cylindrical samples Ga0, Ga0.75, Ga1.0, and Ga1.25 with 3.5 mm in diameter and 7 mm in length.

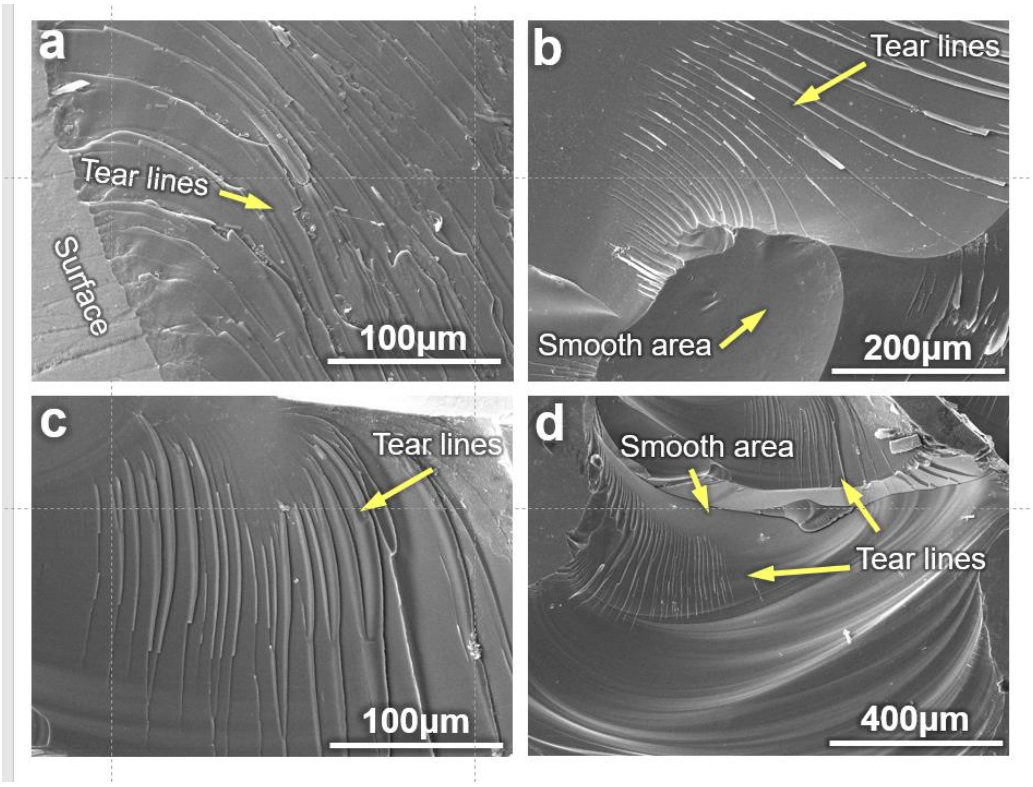

Fig. XXX5 SEM images of the fractured surfaces of cylindrical Mg-Zn-Ca-Ga BMG samples (a) Ga0, (b) Ga0.75, (c) Ga1.0 and (d)Ga1.25 after the compressive test.

3.3 Electrochemical behavior

The OCP curves of Mg-Zn-Ca-Ga metallic glass ribbons with ~~the variation of~~ Ga ~~addition~~ content are presented in Fig. XXX6(a). The OCP value of the metallic glasses ~~increase toward~~ moves in the ~~positive potential~~ noble direction in the first 600 s, which may result ~~in~~ from the formation of corrosion product film ~~and accumulation of dissolved metallic ions on the interface of solution/substrate~~. Then ~~they get to~~ the OCP became stable ~~gradually~~ ~~because~~ when the corrosion product film stopped growing eventually ~~is getting in equilibrium with its dissolution and the concentration of dissolved metallic ions getting equilibration~~. With the increase of ~~addition of element~~ Ga, the OCP value ~~of all metallic glass~~ increases from about -1.4 to -1.1 V as shown in Fig. XXX6(a), which can be ascribed to the relatively higher electrode potential of ~~element~~ Ga. Meanwhile the addition of Ga may also help forming a dense oxide or hydroxide film on~~to~~ the metallic glasses.

After 60 min OCP test, electrochemical impendence spectroscopy (EIS) measurement was conducted in Hanks' solution at each OCP to investigate the corrosion resistance of Mg-Zn-Ca-Ga metallic glass samples with different content of Ga, and the test result is presented in Fig. XXX6(b). To better understand the corrosion behaviors of different metallic glass samples, the electrical equivalent circuit (EEC, as shown in Fig. XXX6(d) with two-time constants was applied to fit the EIS result. On account of the the time-constant dispersion [28] caused by surface heterogeneity [29][30], fractal geometry[31][32], electrode porosity[33][34], variation of coating and surface composition [35][36], two-dimensional (2D) and three-dimensional (3D) distribution[36], and geometry-induced current and potential distributions [37][38][39], the constant phase element (*CPE*) was introduced[30][40] to fit the EIS data. In the EEC model, R_s is the solution resistance generated between WE and RE, R_f and CPE_f

are the resistance and capacitance of the corrosion product film on the metallic glasses, CPE_{dl} is the capacitance of the electrical double layer generated on the metallic glass, R_{ct} is charge transfer resistance of the metallic glass. The parameters including R_s, R_f, CPE_f, CPE_{dl}, R_{ct}, and R_p (polarization resistance) fitted by the EEC in Fig. XXX6(d) are listed in Table TTT3. Compared with crystalline Mg alloy, there is no inductive loop on the Nyquist plots at low-frequency as shown in Fig. XXX6(b), suggesting that the addition of element Zn, Ca and Ga into the alloy directly improves the corrosion resistance of the alloy and effectively restrains severe corrosion forming. Without any Ga added into the metallic glass, sample Ga0 has the smallest capacitive loop and its R_p is only 3618 Ω cm^2. With the addition of Ga from 0.25 at.% to 1.25 at.%, the values of R_p increase gradually from 4467 Ω cm^2 to 20282 Ω cm^2.

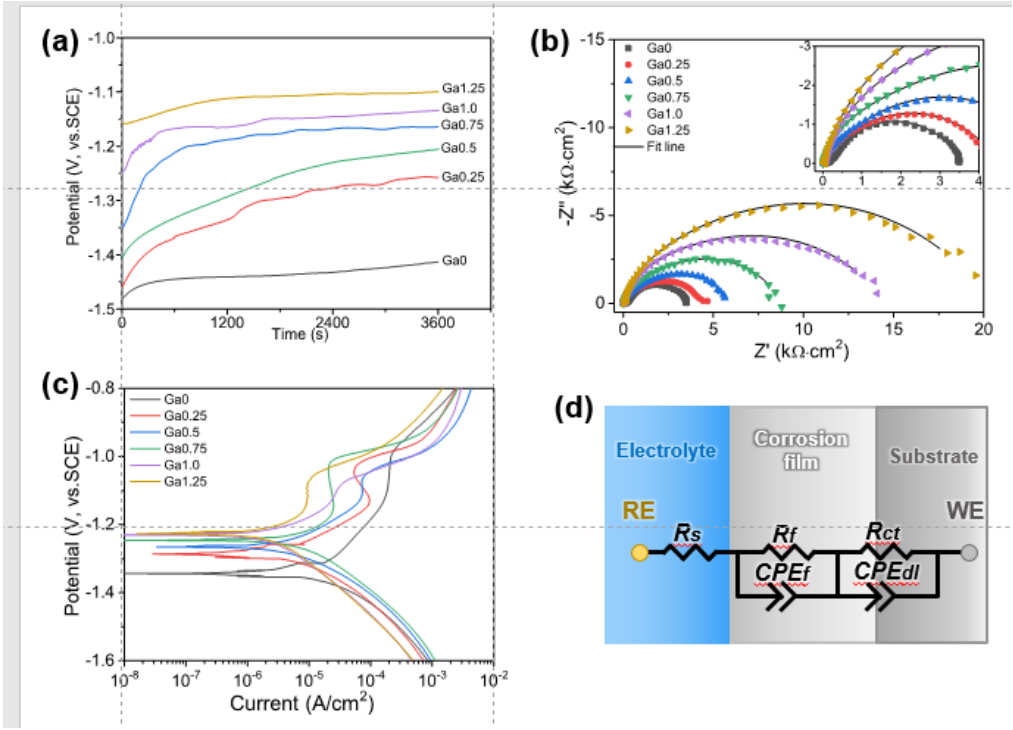

Fig.XXX6 (a) Open circuit potential (OCP) curves, (b) Nyquist plots and (c) potential dynamic polarization (PDP) curves of different Mg-Zn-Ca-Ga metallic glasses (Ga0,

Ga0.25, Ga0.5, Ga0.75, Ga1.0, and Ga1.25) tested in hanks' solution at 37°C. And (d) electrical equivalent circuit (EEC) used in the fitting of EIS result.

Table TTT3

The parameters obtained after fitting of Nyquist plots in Fig. XXX6(b).

EIS parameters	Units	Ga0	Ga0.25	Ga0.5	Ga0.75	Ga1.0	Ga1.25
R_s	Ω cm^2	30	16	15	14	66	45
CPE_f	Ω^{-1}cm^{-2}s^n	3.74 e-5	1.52 e-5	1.52 e-5	1.04 e-5	5.83 e-6	6.54 e-6
n_f		0.866	0.878	0.869	0.901	0.891	0.899
R_f	Ω cm^2	315	949	1182	2691	4559	5712
CPE_{dl}	Ω^{-1}cm^{-2}s^n	13.0 e-5	7.37 e-5	6.92 e-5	5.88 e-5	3.97 e-5	3.18 e-5
n_{dl}		0.847	0.627	0.635	0.671	0.589	0.606
R_{ct}	Ω cm^2	3303	3518	4769	6080	9929	14570
R_p	Ω cm^2	3618	4467	5951	8771	14488	20282

Fig. XXX6(c) shows the PDP curves of Mg-Zn-Ca-Ga metallic glasses, and the corresponding fitting result is presented in Table TTT4. By analyzing the result of the PDP curves of all metallic glasses, it can be observed that sample Ga0 has the lowest E_{corr} (-1.343 V), E_{corr} increases from -1.281 V to -1.225 V gradually with the addition of element Ga. The increase of E_{corr} coincides with the test result of OCP. With the addition of Ga, obvious passivation phenomenon appears on the PDP curves at about -1.1 V. And i_{corr} decreases from 18.8 μA/cm^2 to 2.5 μA/cm^2 with the addition of Ga from 0 to 1.25at.%, which is coincidence with the fitting result of EIS data according to the Stern-Geary equation[41].

$$R_p = \frac{b_a \cdot b_c}{2.3(b_a + b_c) \cdot i_{corr}} \qquad (2)$$

Table TTT4

Fitting result of PDP curves in Fig. XXX6(c).

Parameters	Units	Ga0	Ga0.25	Ga0.5	Ga0.75	Ga1.0	Ga1.25
E_{corr}	V vs. SCE	-1.343	-1.281	-1.264	-1.243	-1.229	-1.225

I_{corr}	μA/cm^2	18.8	9.1	6.3	3.5	2.9	2.5
$-b_c$	mV/dec	158	134	121	132	155	143
b_a	mV/dec	287	130	128	123	116	86

3.3 Immersion test

Fig. XXX7 shows the surface morphologies of Mg-Zn-Ca-Ga metallic glass samples after 48 h immersion in Hanks' solution at 37℃. After the immersion test, obvious filiform corrosion (indicated by arrows) and pitting corrosion spots appear on the surfaces of sample Ga0 (Fig. XXX7(a1)(a2)), Ga0.25 (Fig. XXX7(b1)(b2)), and Ga0.5 (Fig. XXX7(c1)(c2)). Pitting corrosion, as the main corrosion form of Mg-based metallic glasses, was always observed in Mg-Zn-Ca based [21] and Mg-Cu-Y-Zn [42] metallic glasses, and filiform corrosion was also reported in of Mg-Cu-Ni-Ag-Zn-Gd-Y BMG [43]. With 0.5 at.% addition of element Ga, exfoliation of corrosion film appears on the corrosion surface of Ga0.5 (Fig. (c1)(c2)). With the further increase of Ga in the metallic glasses, the inclination of filiform and pitting corrosion reduced, and the metallic glass tends to uniform corrosion. Meanwhile, the larger amount of exfoliation of corrosion film appears on the surface of metallic glasses. Combining with the analysis of the electrochemical test results, the addition of Ga can promote the formation of passivation corrosion product film on the surface and effectively improve the anti-corrosion performance of the Mg-Zn-Ca-Ga metallic glass.

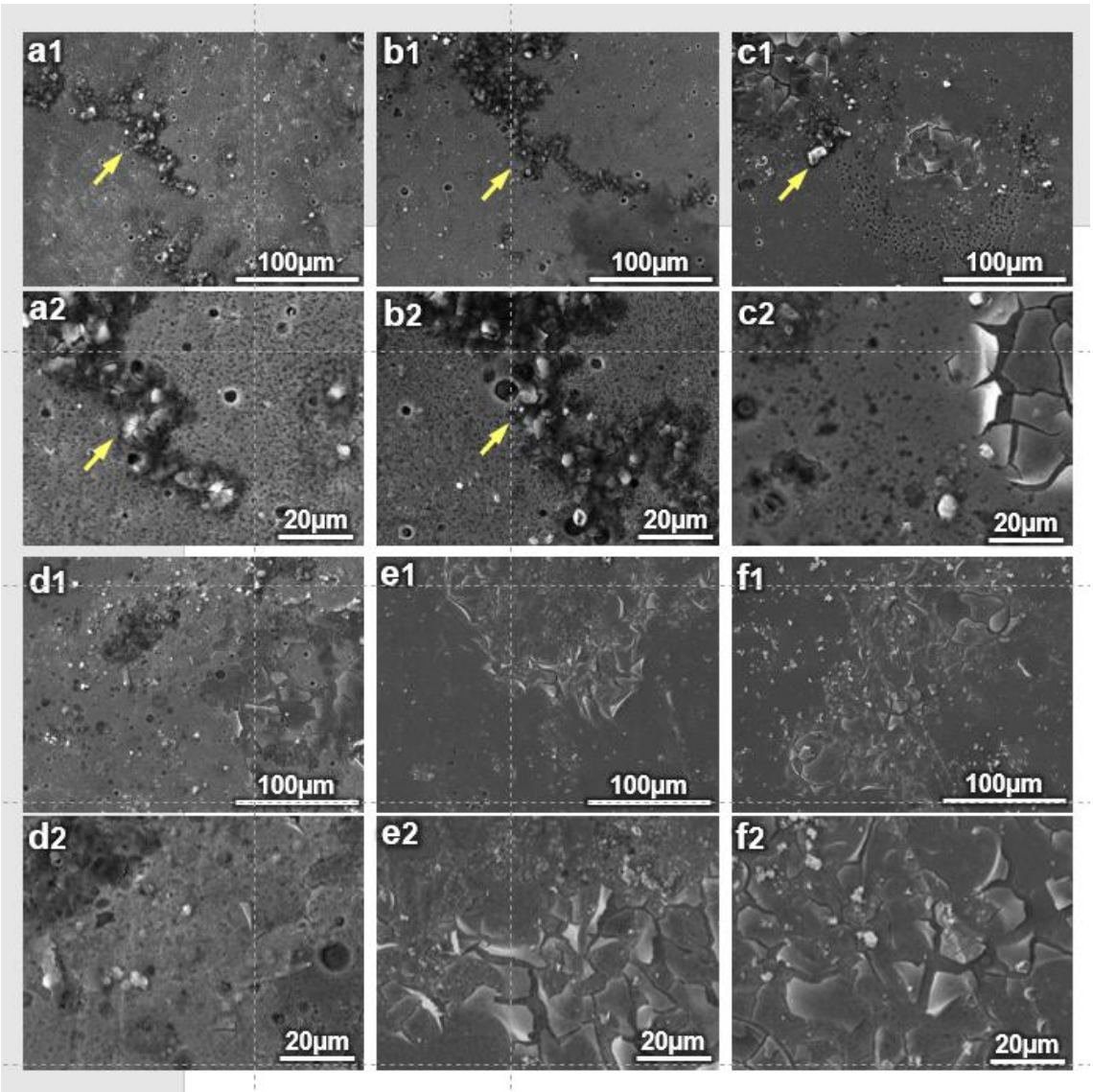

Fig. XXX7 Surface morphologies of Mg-based metallic glasses of (a1)(a2) Ga0, (b1)(b2) Ga0.25, (c1)(c2) Ga0.5, (d1)(d2) Ga0.75, (e1)(e2) Ga1.0, and (f1)(f2) Ga1.25 after 48h immersion in Hanks' solution at 37°C.

4. Discussion

4.1 Corrosion mechanism

To investigate the relationship between the element Ga and passivation phenomenon of the corrosion product film of the metallic glass, Pilling-Bedworth ratio [44] of oxide

(PBR_O, Eq. (3)) and hydroxide (PBR_{OH}, Eq. (4)) were introduced to evaluate the compactness and anti-corrosion performance of the corrosion product film on the metallic glass substrate. In Eqs. (3) and (4), V_M is the volume of a unit mass of pure metal, V_O and V_{OH} is the corresponding volume of the metallic oxide and metallic hydroxide of a unit mass of pure metal respectively. The parameters of related oxides and hydroxides are listed in Table TTT5 reference to Lange's handbook of chemistry[45], and the calculated PBR_O and PBR_{OH} are listed in Table TTT6. By the comparison of PBR_O of Mg, Zn, Ca and Ga, the oxidation of Zn and Ga can help form a more dense oxide film on the metallic substrate than that of Mg and Ca because the PBR_O of Zn and Ga (1.585 and 1.226) are significantly larger than that of Mg and Ca (0.806 and 0.657). Meanwhile, the values of PBR_{OH} of Mg, Zn, Ca and Ga were taken into account, because their hydroxides play more important roles in the corrosion process in aqueous solution. On the one hand, PBR_{OH} of Zn and Ga (3.554 and 2.67) are obviously larger than that of Mg and Ca (1.769 and 1.275). And on the other hand, the values of K_{sp} of $Zn(OH)_2$ and $Ga(OH)_3$ are several order of magnitude less than that of $Mg(OH)_2$ and $Ca(OH)_2$, indicating that $Zn(OH)_2$ and $Ga(OH)_3$ are more stable and insoluble in aqueous solution. Therefore the addition of Zn or Ga can effectively help to form more protective corrosion product film on the metallic glass substrate and therefore improve the corrosion resistance.

$$PBR_O = \frac{V_O}{V_M} \qquad (3)$$

$$PBR_{OH} = \frac{V_{OH}}{V_M} \qquad (4)$$

Table TTT5

Parameters of oxides and hydroxides of Mg, Zn, Ca and Ga at room temperature[45].

	Molecular weight	Density (g/cm^3)	pK_{sp}	K_{sp}
$Mg(OH)_2$	58.32	2.360	11.25	5.61×10^{-12}
$Zn(OH)_2$	99.40	3.053	16.5	3×10^{-17}
$Ca(OH)_2$	74.09	2.248	5.26	5.5×10^{-6}
$Ga(OH)_3$	120.74	3.84*	35.14	7.28×10^{-36}
MgO	40.30	3.580	––	––
ZnO	81.38	5.606	––	––
CaO	56.08	3.300	––	––
Ga_2O_3 (α)	187.44	6.480	––	––

* The density value of $Ga(OH)_3$ is obtained from the standard diffraction pattern (JCSDS card NO. 18-0532).

Table TTT6

Density, PBR_{OH}, and PBR_O of pure metallic Mg, Zn, Ca and Ga.

	Pure Mg	Pure Zn	Pure Ca	Pure Ga
Density (g/cm^3)	1.74	7.14	1.55	5.91
PBR_O	0.806	1.585	0.657	1.226
PBR_{OH}	1.769	3.554	1.275	2.67

For ordinary crystalline Mg-based alloys such as Mg-Al, Mg-Zn, and Mg-Re alloy, they always suffered from severe corrosion in common electrolyte solutions, and dramatically rapid corrosion and the phenomenon of anodic hydrogen evolution are often observed at their anodic region during the PDP tests[46]. Compared with common Mg alloy, Mg-Zn-Ca-Ga metallic glass shows outstanding anti-corrosion resistance, and the passivation phenomenon was observed in their anodic region as shown in Fig. XXX7(c). The excellent corrosion performance of Mg-Zn-Ca-Ga metallic glass could be explained by its simplified polarization diagram (Fig. XXX8(a)) and the related electrochemical reactions of different elements are expressed in Eqs.(5)(6)(7)(8)(9). To simplify the analyzation process, elements of Mg, Zn, Ca and Ga are classified into two

categories including active metal elements (Mg and Ca) and inactive metal elements (Zn and Ga). As shown in Fig. XXX8 (a), the green dash lines correspond the cathodic reaction ($I_{H+/H2}$, Eq. (5)) and anodic reactions ($I_{(Mg/Ca),e}$, Eqs. (6)(7)) of Mg and Ca, the red lines ($I'_{H+/H2}$ and $I'_{(Zn/Ga),e}$) correspond the cathodic reaction (Eq. (5)) and anodic reactions of Zn and Ga (Eqs. (8)(9)). When the applied potential (E) lower than the self-corrosion potential of Mg/Ca ($E_{(Mg/Ca)}$), as shown in Fig. XXX(b1), the cathodic reaction generates on the surface of elements Zn/Ga more than Mg/Ca, because the cathodic current density of Zn/Ga is higher than that of Mg/Ca. When $E_{Mg/Ca} < E < E_{Zn/Ga}$, corresponding to the illustration Fig. XXX(b2), Ca is oxidized into Ca^{2+} and dissolved into the electrolyte, and Mg is oxidized into loose $Mg(OH)_2$ film. When $E_{Mg/Ca} < E < E_b$, because the anodic current density of Zn/Ga ($I'_{(Zn/Ga),e}$) is larger than its cathodic current density ($I'_{H+/H2}$), Zn and Ga are oxidized into $Zn(OH)_2$ and $Ga(OH)_3$. And combining with $Mg(OH)_2$, $Zn(OH)_2$ and $Ga(OH)_3$ form into a dense protective film which inhibits the anodic reactions of different elements ($I'_{(Zn/Ga),e}$ and $I_{(Mg/Ca),e}$) and form the passivation potential region(ΔE) as shown in Fig. XXX(b3). When the furtherly increased E is larger than the breakdown potential (E_b), as shown in Fig. XXX8(b4), the passivation film breaks down and the electrochemical reaction gets into the Tafel linear region of whole metallic glass ($I_{(BMG),e}$).

Cathodic reaction	$2H_2O + 2e^- \rightarrow H_2 + 2OH^-$	(5)
Anodic reaction 1	$Mg + 2H_2O \rightarrow Mg(OH)_2 + 2H^+ + 2e^-$	(6)
Anodic reaction 2	$Ca \rightarrow Ca^{2+} + 2e^-$	(7)
Anodic reaction 3	$Zn + 2H_2O \rightarrow Zn(OH)_2 + 2H^+ + 2e^-$	(8)
Anodic reaction 4	$Ga + 3H_2O \rightarrow Ga(OH)_3 + 2H^+ + 3e^-$	(9)

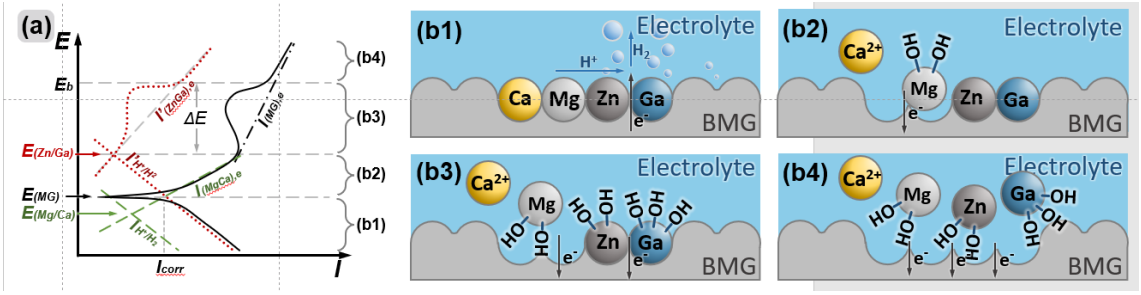

Fig. XXX8 Mechenesim of passivation: (a) Polarization diagram of MgZnCaGa BMG and the corresponding schematic diagram of electrochemical reactions on the BMG surface when (b1) $E < E_{Mg/Ca}$, (b2) $E_{Mg/Ca} < E < E_{Zn/Ga}$, (b3) $E_{Zn/Ga} < E < E_b$ and (b4) $E_b < E$.

4.2 Relationship between GFA and binary phase diagrams

In this study, a new theory to design the composition of BMG was proposed by analyzing the binary phase diagrams of each two elements. Firstly a hypothesis should be established, as indicated by the arrow in Fig. XXX9(a), the composition inhomogeneity of alloy increases with the macroscopic concentration changing to the microcosmic concentration. Fig. XXX9(b) shows a kind of binary phase diagram on which the left side is phase α and the right side is intermetallic phases of β1 and β2. With the decrease of temperature from T1 to T3, as shown in Fig. XXX9(c1)(c2)(c3), the tops of Gibbs curves of phase α, β1 and β2 get below the Gibbs curve of liquid. As we all know, the eutectic composition can get the balance of phase α and β1 during the process of equilibrium solidification, and eutectic composition has a shorter temperature region of liquid-solid two-phase during the solidification[23] [????]. The composition near phases of intermetallics (like β1 and β2) may provide higher GFA during the process of quick solidification [23][???]. On the one hand, compared with β1 and β2, phase α has larger solubility which always corresponds to simple crystal structure and

the easiness of crystalization. On the other hand, the composition near c β2 may make more chances of formation of clusters with similar complex structures of phase β1 and β2 from the supercooled liquid phase. Therefore the more intermetallic phases like β1 and β2 near the sides of the eutectic point, the higher GFA may the alloy has.

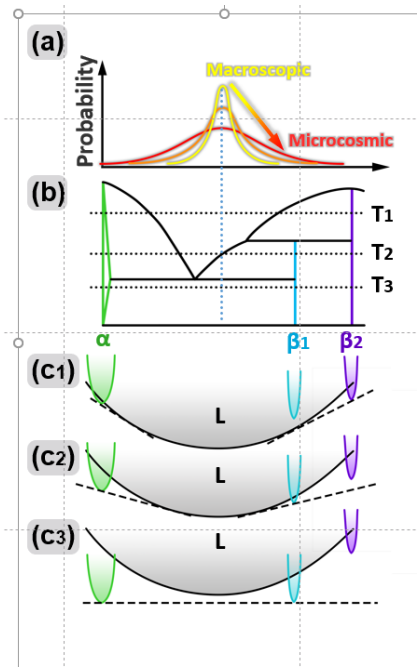

Fig. XXX9. (a) Probability distribution diagram of macroscopic concentration and microcosmic concentration, (b) one kind of binary phase diagram and diagrams containing Gibbs free energy curves of all phases at different temperatures: (c1) T1, (c2) T2 and (c3) T3.

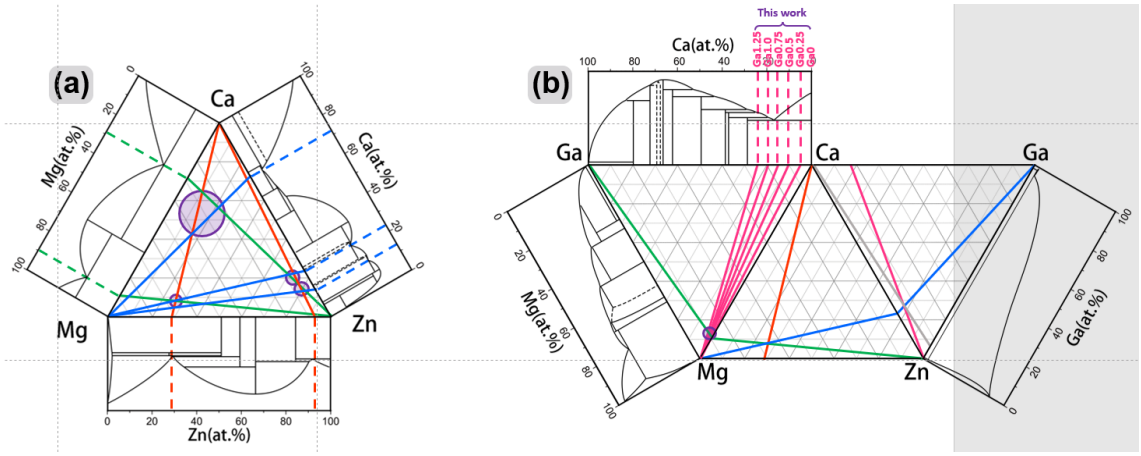

Fig. XXX10 (a) phase diagram of Mg, Zn and Ca, (b) phase diagram of Mg, Zn, Ca and Ga.

Even though there are many theories were proposed to predict and investigate the relationship between composition and GFA, few theories were proposed depending on binary phase diagrams. As shown in Fig. XXX10 (a), the eutectic compositions are indicated by dash lines in binary diagrams, and diagonal lines of the eutectic composition of Mg, Zn and Ca are depicted by straight lines. Three diagonal lines of Mg, Zn and Ca form triangle regions as indicated by circles in which the composition of each couple elements nears its eutectic point. Intersection points of diagonal lines near the Mg side indicated by a small circle was found to form the Mg-based BMGs[47][48][49][50][51]. And the regions in circles near Zn-rich and Ca-rich were also found Zn-based BMGs [52] and Ca-based BMGs [53][54][53][55][56] respectively.

The composition of Mg-Zn-Ca-Ga BMGs studied in this paper are indicated by a small circle shown in Fig. XXX10(b). Generally speaking, as the microalloying element, Ga should increase or decrease the GFA gradually with its addition. Whereas with the addition of Ga from 0 to 1.25 at.%, the D_c of Mg-Zn-Ca-Ga BMG decreased sharply to 0.5mm and then increased to the maximum D_c 5mm at the addition of 1 at.% Ga which corresponded to the eutectic composition in the Ca-Ga phase diagram(Fig. XXX10(b)). Therefore the relationships between each couple of elements (binary phase diagrams) play an important role in the GFA of the alloy system.

5. Conclusion

1. With the addition of 1 at.% Ga, Mg-Zn-Ca-Ga metallic glass got the highest GFA and the critical diameter (D_c) reached 5 mm.

2. With the improvement of GFA and the addition of alloying element Ga, the fracture strength of Mg-Zn-Ca-Ga bulk metallic glasses was slightly improved.

3. With the increase of Ga addition, Mg-Zn-Ca-Ga metallic glasses had obvious higher free-corrosion potential and lower corrosion current density corresponding higher corrosion resistance. And the addition of element Ga can help form dense corrosion product film and directly improve the corrosion performance.

Acknowledgments

The work described in this paper was supported by the National Natural Science Foundation of China (Grant No. 31070841, 51705195).

References

[1] A. Inoue, A. Takeuchi, Recent development and application products of bulk glassy alloys, Acta Mater. 59 (2011) 2243–2267. doi:10.1016/j.actamat.2010.11.027.

[2] W. Klement, R.H. Willens, P. Duwez, Non-crystalline structure in solidified Gold-Silicon alloys, Nature. (1960). doi:10.1038/187869b0.

[3] A. Inoue, C. Suryanarayana, Bulk metallic glasses, 2011.

[4] A. Takeuchi, A. Inoue, Classification of BulkMetallic Glasses By Atomic Size Difference, Heat of Mixing and Period of Constituent Elements and Its

Application To Characterization of the Main Alloying Element, Mater. Trans. 46 (2005) 2817–2829. doi:10.2320/matertrans.46.2817.

[5] A. Inoue, N. Nishiyama, H. Kimura, Preparation and thermal stability of Bulk Amorphous Pd40Cu30Ni10P20 alloy cylinder of 72 mm in diameter, Mater. Trans. 38 (1997) 179–183. doi:10.1016/S0022-3093(03)00006-1.

[6] C.L. Qiu, Q. Chen, L. Liu, K.C. Chan, J.X. Zhou, P.P. Chen, S.M. Zhang, A novel Ni-free Zr-based bulk metallic glass with enhanced plasticity and good biocompatibility, Scr. Mater. 55 (2006) 605–608. doi:10.1016/j.scriptamat.2006.06.018.

[7] C.L. Qin, J.J. Oak, N. Ohtsu, K. Asami, A. Inoue, XPS study on the surface films of a newly designed Ni-free Ti-based bulk metallic glass, Acta Mater. 55 (2007) 2057–2063. doi:10.1016/j.actamat.2006.10.054.

[8] Z. Liu, K.C. Chan, L. Liu, Development of Ni- and Cu-Free Zr-Based Bulk Metallic Glasses for Biomedical Applications, Mater. Trans. 52 (2011) 61–67. doi:10.2320/matertrans.M2010068.

[9] H.F. Li, Y.F. Zheng, Recent advances in bulk metallic glasses for biomedical applications, Acta Biomater. 36 (2016) 1–20. doi:10.1016/j.actbio.2016.03.047.

[10] M.S. Dambatta, S. Izman, B. Yahaya, J.Y. Lim, D. Kurniawan, Mg-based bulk metallic glasses for biodegradable implant materials: A review on glass forming ability, mechanical properties, and biocompatibility, J. Non. Cryst. Solids. 426 (2015) 110–115. doi:10.1016/j.jnoncrysol.2015.07.018.

[11] M.P. Staiger, A.M. Pietak, J. Huadmai, G. Dias, Magnesium and its alloys as orthopedic biomaterials: A review, Biomaterials. 27 (2006) 1728–1734.

doi:10.1016/j.biomaterials.2005.10.003.

[12] W.H. Wang, C. Dong, C.H. Shek, Bulk metallic glasses, Mater. Sci. Eng. R Reports. 44 (2004) 45–89. doi:10.1016/j.mser.2004.03.001.

[13] J.R. Scully, A. Gebert, J.H. Payer, Corrosion and related mechanical properties of bulk metallic glasses, J. Mater. Res. 22 (2007) 302–313. doi:10.1557/jmr.2007.0051.

[14] R. Nowosielski, K. Cesarz-Andraczke, Impact of Zn and Ca on dissolution rate, mechanical properties and GFA of resorbable Mg–Zn–Ca metallic glasses, Arch. Civ. Mech. Eng. 18 (2018) 1–11. doi:10.1016/j.acme.2017.05.009.

[15] X. Gu, Y. Zheng, S. Zhong, T. Xi, J. Wang, W. Wang, Corrosion of, and cellular responses to Mg-Zn-Ca bulk metallic glasses, Biomaterials. 31 (2010) 1093–1103. doi:10.1016/j.biomaterials.2009.11.015.

[16] B. Zberg, P.J. Uggowitzer, J.F. Löffler, MgZnCa glasses without clinically observable hydrogen evolution for biodegradable implants, Nat. Mater. 8 (2009) 887–891. doi:10.1038/nmat2542.

[17] H. Ma, L.L. Shi, J. Xu, Y. Li, E. Ma, Discovering inch-diameter metallic glasses in three-dimensional composition space, Appl. Phys. Lett. 87 (2005) 1–3. doi:10.1063/1.2126794.

[18] H. Li, S. Pang, Y. Liu, P.K. Liaw, T. Zhang, In vitro investigation of Mg-Zn-Ca-Ag bulk metallic glasses for biomedical applications, J. Non. Cryst. Solids. 427 (2015) 134–138. doi:10.1016/j.jnoncrysol.2015.07.043.

[19] S. González, E. Pellicer, J. Fornell, A. Blanquer, L. Barrios, E. Ibáñez, P. Solsona, S. Suriñach, M.D. Baró, C. Nogués, J. Sort, Improved mechanical

performance and delayed corrosion phenomena in biodegradable Mg-Zn-Ca alloys through Pd-alloying, J. Mech. Behav. Biomed. Mater. 6 (2012) 53–62. doi:10.1016/j.jmbbm.2011.09.014.

[20] Y. Zhao, J. Zhu, L. Chang, J. Song, X. Chen, X. Hui, Influence of Cu content on the mechanical properties and corrosion resistance of Mg-Zn-Ca bulk metallic glasses, Int. J. Miner. Metall. Mater. 21 (2014) 487–493. doi:10.1007/s12613-014-0933-6.

[21] H. Li, S. Pang, Y. Liu, L. Sun, P.K. Liaw, T. Zhang, Biodegradable Mg-Zn-Ca-Sr bulk metallic glasses with enhanced corrosion performance for biomedical applications, Mater. Des. 67 (2015) 9–19. doi:10.1016/j.matdes.2014.10.085.

[22] J.H. Hanks, Hanks' balanced salt solution and pH control - Springer, Methods Cell Sci. (1975). http://www.springerlink.com/index/P214662317R6810J.pdf.

[23] D. Turnbull, Under What Conditions Can A Glass Be Formed?, Contemp. Phys. 10 (1969) 473–488. doi:10.1080/00107516908204405.

[24] Z.P. Lu, C.T. Liu, A new glass-forming ability criterion for bulk metallic glasses, Acta Mater. 50 (2002) 3501–3512. doi:10.1016/S1359-6454(02)00166-0.

[25] A. Inoue, Stabilization of metallic supercooled liquid and bulk amorphous alloys, Acta Mater. 48 (2000) 279–306. doi:10.1016/S1359-6454(99)00300-6.

[26] Z.P. Lu, Y. Li, S.C. Ng, Reduced glass transition temperature and glass forming ability of bulk glass forming alloys, J. Non. Cryst. Solids. 270

(2000) 103–114. doi:10.1016/S0022-3093(00)00064-8.

[27] K.F. Shamlaye, K.J. Laws, J.F. Löffler, Exceptionally broad bulk metallic glass formation in the Mg–Cu–Yb system, Acta Mater. 128 (2017) 188–196. doi:10.1016/j.actamat.2017.02.013.

[28] M.E. Orazem, B. Tribollet, Electrochemical Impedance Spectroscopy, 2008. doi:10.1002/9780470381588.

[29] H. Fricke, XXXIII. The theory of electrolytic polarization , London, Edinburgh, Dublin Philos. Mag. J. Sci. (1932). doi:10.1080/14786443209462064.

[30] G.J. Brug, A.L.G. van den Eeden, M. Sluyters-Rehbach, J.H. Sluyters, The analysis of electrode impedances complicated by the presence of a constant phase element, J. Electroanal. Chem. 176 (1984) 275–295. doi:10.1016/S0022-0728(84)80324-1.

[31] L. Nyikos, T. Pajkossy, Fractal dimension and fractional power frequency-dependent impedance of blocking electrodes, Electrochim. Acta. (1985). doi:10.1016/0013-4686(85)80016-5.

[32] B. Sapoval, Linear and non-linear behavior of fractal and irregular electrodes, Solid State Ionics. (1995). doi:10.1016/0167-2738(94)00171-N.

[33] DELAHAY ED P, TOBIAS ED CW, ADVANCES IN ELECTROCHEMISTRY AND ELECTROCHEMICAL ENGINEERING, V 7, ELECTROCHEMISTRY, Intersci. Publ, Div John Wiley Sons, Inc. (1970). doi:10.1016/s0003-2670(01)80292-0.

[34] R. De Levie, Electrochemical response of porous and rough electrodes, Adv. Electrochem. Electrochem. Eng. 6 (1967) 329–397.

[35] J. Vogelsang, W. Strunz, The evaluation of experimental dielectric

data of barrier coatings by means of different models, Electrochim. Acta. (2001). doi:10.1016/S0013-4686(01)00644-2.

[36] J.B. Jorcin, M.E. Orazem, N. Pébère, B. Tribollet, CPE analysis by local electrochemical impedance spectroscopy, in: Electrochim. Acta, 2006. doi:10.1016/j.electacta.2005.02.128.

[37] J. Newman, Current Distribution on a Rotating Disk below the Limiting Current, J. Electrochem. Soc. (1966). doi:10.1149/1.2423795.

[38] M.E. Orazem, P. Agarwal, L.H. Garcia-Rubio, Critical issues associated with interpretation of impedance spectra, J. Electroanal. Chem. (1994). doi:10.1016/0022-0728(94)87056-X.

[39] M. Durbha, A Mathematical Model for the Radially Dependent Impedance of a Rotating Disk Electrode, J. Electrochem. Soc. (1999). doi:10.1149/1.1391914.

[40] P. Zoltowski, On the electrical capacitance of interfaces exhibiting constant phase element behaviour, J. Electroanal. Chem. (1998). doi:10.1016/S0022-0728(97)00490-7.

[41] F. Mokhtarian, A.K. Mackworth, A theory of multiscale, curvature-based shape representation for planar curves, IEEE Trans. Pattern Anal. Mach. Intell. (1992). doi:10.1109/34.149591.

[42] X.L. Zhang, G. Chen, T. Bauer, Mg-based bulk metallic glass composite with high bio-corrosion resistance and excellent mechanical properties, Intermetallics. (2012). doi:10.1016/j.intermet.2012.04.018.

[43] A. Gebert, V. Haehnel, E.S. Park, D.H. Kim, L. Schultz, Corrosion behaviour of Mg65Cu7.5Ni7.5Ag5Zn5Gd5Y5 bulk metallic glass in aqueous

environments, Electrochim. Acta. (2008). doi:10.1016/j.electacta.2007.12.001.

[44] N.B. Pilling, The oxidation of metals at high temperature, J. Inst. Met. 29 (1923) 529–582.

[45] J.G. Speight, Lange's Handbook Of Chemistry, 16th ed., 2005.

[46] S. Thomas, N. V. Medhekar, G.S. Frankel, N. Birbilis, Corrosion mechanism and hydrogen evolution on Mg, Curr. Opin. Solid State Mater. Sci. (2015). doi:10.1016/j.cossms.2014.09.005.

[47] Y.Y. Zhao, X. Zhao, Structural relaxation and its influence on the elastic properties and notch toughness of Mg-Zn-Ca bulk metallic glass, J. Alloys Compd. 515 (2012) 154–160. doi:10.1016/j.jallcom.2011.11.125.

[48] Y.F. Zhao, D.Y. Lin, X.H. Chen, Z.K. Liu, X.D. Hui, Sluggish mobility and strong icosahedral ordering in Mg-Zn-Ca liquid and glassy alloys, Acta Mater. 67 (2014) 266–277. doi:10.1016/j.actamat.2013.12.037.

[49] J. Wang, S. Huang, Y. Li, Y. Wei, X. Xi, K. Cai, Microstructure, mechanical and bio-corrosion properties of Mn-doped Mg-Zn-Ca bulk metallic glass composites, Mater. Sci. Eng. C. (2013). doi:10.1016/j.msec.2013.05.020.

[50] Q.F. Li, H.R. Weng, Z.Y. Suo, Y.L. Ren, X.G. Yuan, K.Q. Qiu, Microstructure and mechanical properties of bulk Mg-Zn-Ca amorphous alloys and amorphous matrix composites, Mater. Sci. Eng. A. (2008). doi:10.1016/j.msea.2007.10.027.

[51] X. Gu, G.J. Shiflet, F.Q. Guo, S.J. Poon, Mg-Ca-Zn bulk metallic glasses with high strength and significant ductility, J. Mater. Res. (2005). doi:10.1557/JMR.2005.0245.

[52] W. Jiao, K. Zhao, X.K. Xi, D.Q. Zhao, M.X. Pan, W.H. Wang,

Zinc-based bulk metallic glasses, J. Non. Cryst. Solids. 356 (2010) 1867–1870. doi:10.1016/j.jnoncrysol.2010.07.017.

[53] J.D. Cao, N.T. Kirkland, K.J. Laws, N. Birbilis, M. Ferry, Ca-Mg-Zn bulk metallic glasses as bioresorbable metals, Acta Biomater. (2012). doi:10.1016/j.actbio.2012.03.009.

[54] O.N. Senkov, J.M. Scott, Formation and thermal stability of Ca-Mg-Zn and Ca-Mg-Zn-Cu bulk metallic glasses, Mater. Lett. 58 (2004) 1375–1378. doi:10.1016/j.matlet.2003.09.030.

[55] O.N. Senkov, D.B. Miracle, V. Keppens, P.K. Liaw, Development and characterization of low-density Ca-based bulk metallic glasses: An overview, in: Metall. Mater. Trans. A Phys. Metall. Mater. Sci., 2008. doi:10.1007/s11661-007-9334-z.

[56] O.N. Senkov, D.B. Miracle, J.M. Scott, Development and characterization of Ca-Mg-Zn-Cu bulk metallic glasses, Intermetallics. 14 (2006) 1055–1060. doi:10.1016/j.intermet.2006.01.024.